Effects of azimuthal and radial spreads of canonical momentum on electron-beam focusing characteristics in the presence of space-charge forces

Moshe Cohen[a)] and Avraham Gover
Department of Electrical Engineering–Physical Electronics, Faculty of Engineering, Tel-Aviv University, Ramat-Aviv 69978, Israel

(Received 14 November 1994; accepted for publication 17 February 1995)

A theoretical and numerical investigation of the effects of azimuthal and radial spreads of canonical momentum on an electron beam focused by a magnetic lens in the presence of space-charge forces is presented. The particles are inserted with an initial Gaussian distribution in the transverse space and in the momentum coordinates or with a uniform initial current distribution. The particle trajectory equation is derived for parameters of an arbitrary applied fields configuration with cylindrical symmetry, and a nonvanishing initial canonical momentum. In the absence of an initial momentum spread particles launched above a critical radial distance from the axis exhibit a *phase-space tearing* effect in the electron distribution. The inclusion of initial canonical momentum spread in the model allows for skewed trajectories with strong centrifugal force which prevents the appearance and overshadows the effect of strong space-charge forces near the axis, which are responsible for the phase-space tearing effect. © *1995 American Institute of Physics.*

I. INTRODUCTION

For many applications such as microwave tubes,[1] free-electron lasers (FELs),[2] high-energy injector linacs,[3] and others, a low-emittance high intensity beam is an essential requirement. For FEL experiments, the e-beam is preaccelerated, bunched, focused, then matched to the main acceleration section in order to inject it into the wiggler.[4] The beam quality requirements inside the wiggler are in general very stringent: the beam in the low-energy section is typically dominated by space-charge forces. Electron-beam transport through this section may spoil the beam quality as evidenced by emittance growth due to space-charge forces; this limits the gain that can be expected for a given set of parameters. In many cases the beam emittance could play a significant role in the device behavior. Azimuthal and radial spreads of the canonical momentum that were generated close to the cathode influence the individual electron trajectories. This effect yields subsequent current-density phase-space distributions which differ from those estimated by models which do not consider these spreads. A model based on particle equations of motion which are used to derive the particle trajectories for a general field structure is presented in this paper. The present treatment considers the problem of a continuous, azimuthally symmetrical beam taking into account azimuthal and radial spreads of canonical momentum and space-charge forces. This is an extension of conventional models which consider the phase-space coordinates (r,p_r) only. Here we also allow a spread in the azimuthal momentum p_θ. We introduce also a method of treating the space-charge forces for any given particle distribution. This model permits analysis of a beam with any initial charge distribution and therefore can be used to study the emittance growth problem. Focusing of an e-beam with an initial uniform distribution or Gaussian distribution is studied as an example. Electron trajectories, phase space, and current-density evolution are presented and compared for both distribution functions.

[a)]Electronic mail: moshec@eng.tau.ac.il

II. EQUATIONS OF MOTION

The motion of an electron is governed by the Lorentz force equation

$$\dot{\mathbf{p}} = -e(\mathbf{E}+\mathbf{v}\times\mathbf{B}), \tag{1}$$

where $\mathbf{p}=\gamma m\mathbf{v}$ is the relativistic kinetic momentum and m is the electron rest mass. The total normalized energy of the electron is given by

$$\gamma=(1-\beta^2)^{-1/2}, \tag{2}$$

with $\beta=|\mathbf{v}|/c$, where $\mathbf{v}$ is the electron velocity and c is the speed of light in vacuum. Here and throughout this paper, the overdot denotes derivative with respect to t and the prime denotes derivative with respect to z. In this force equation, $\mathbf{E}$ and $\mathbf{B}$ are macroscopic fields that are generated by external coils, charges, and currents.

The radial component of the force equation (1), in cylindrical coordinate system, is

$$\gamma m\ddot{r}-\gamma m r\dot{\theta}^2+\dot{\gamma}m\dot{r}=-e(E_r+r\dot{\theta}B_z+E_r^b-v_zB_\theta^b), \tag{3}$$

where E_r^b and B_θ^b are the electron-beam self-fields.

It is convenient to take z as the independent variable and replace the time derivation by

$$\frac{d}{dt}=v_z\frac{d}{dz}. \tag{4}$$

Using this relation and the axial component of the force Eq. (1) in Eq. (3) results in

$$r''=-\frac{e}{\gamma m v_z^2}(v_zB_zr\theta'+v_zB_rrr'\theta'+E_r^b-v_zB_\theta^b)+r\theta'^2. \tag{5}$$

 0021-8979/95/78(1)/16/9/$6.00

The field components in this equation, B_r and B_z, describe the magnetic (solenoidal) field in the radial and axial dimensions, respectively. These components are applied externally and are functions of r and z.

The angular velocity is obtained from the conservation of the canonical angular momentum,

$$\theta'(r,z)=\frac{eB_z(r,z)}{2\gamma mc\beta_z}+\frac{L_{\theta_0}(r_0)}{\gamma mc\beta_z r^2}, \tag{6}$$

where $L_{\theta_0}(r_0) = p_{\theta_0}r_0 - eB_{z0}(r_0)r_0^2/2$ is the canonical angular momentum at the entrance plane ($z=0$) and r_0 is the radial distance from which the particle is launched. We assume that the electrons in the beam may have nonvanishing initial canonical angular momentum, $L_{\theta_0} \neq 0$. Note that such electrons never cross the beam axis because of the centrifugal force and they follow nonmeridional trajectories (never cross the axis in the rotating Larmor reference frame).

The space-charge fields can be derived straightforwardly by using an assumption of a slow variation of the current density in the axial dimension. The azimuthal magnetic self-field is obtained from the axial component of Ampere's law:

$$B_\theta^b(r,z)=\frac{\mu_0}{r}\int_0^r \xi J_z(\xi,z)d\xi=\frac{\mu_0}{2\pi r}I(r,z), \tag{7}$$

where $I(r,z)$ is the total current contained within a circle of radius r around the z axis:

$$I(r,z)=2\pi\int_0^r \xi J_z(\xi,z)d\xi. \tag{8}$$

The radial electric space-charge field is determined from Gauss' law:

$$E_r^b(r,z)=\frac{1}{\epsilon_0 r}\int_0^r \xi\rho(r,z)d\xi=\frac{I(r,z)}{2\pi\epsilon_0 v_z r}. \tag{9}$$

Substituting the angular velocity from Eq. (6) and the self-fields of the e-beam given by Eqs. (7) and (9) into the radial equation of motion, Eq. (5), yields

$$r''=-\left[\frac{\Omega_L(r,z)}{c\beta_z}\right]^2 r+\left[\frac{L_{\theta_0}}{\gamma mc\beta_z}\right]^2\frac{1}{r^3}-\frac{K(r,z)}{r}, \tag{10}$$

where $\Omega_L(r,z)=eB_z(r,z)/2\gamma mc\beta_z$ is the Larmor frequency, and $K(r,z)$ is the radius dependent e-beam perveance, defined as

$$K(r,z)=\frac{e}{\gamma mc^2\beta_z^2}[E_r^b(r,z)-v_zB_\theta^b(r,z)]r$$

$$=\frac{eI(r,z)}{2\pi\epsilon_0\gamma\gamma_z^2mc^3\beta_z^3}. \tag{11}$$

The first term (Lorentz force) in the rhs of Eq. (10) is a focusing force while the two last terms (the centrifugal and the space-charge forces) are defocusing forces. Equation (10) is a general equation of motion which defines the electron trajectories in the presence of magnetic and space-charge forces of cylindrical symmetry.

III. ELECTRON-BEAM REPRESENTATION

The algorithms used to sample the electron-beam distribution, calculate the self-field forces, and represent the resulting current-density distribution are outlined in this section. Assume that the electron-beam cross section is sampled and represented by N_t macroparticles. The total current to be inserted in Eqs. (10) and (11) which induces fields that act on the ith macroparticle located at r_i is given by

$$I(r_i,z)=\sum_{j=1}^{N_t}\alpha_j(z)I_j, \tag{12}$$

where I_j is the current that is represented by the jth macroparticle located at r_j, and $\alpha_j(z)$ is

$$\alpha_j(z)=\begin{matrix}1, & \text{for } r_j<r_i,\\ 0, & \text{otherwise.}\end{matrix} \tag{13}$$

Consider now an e-beam with an initial uniform current-density distribution in the radial dimension; the total current in the beam cross-section area is divided into a large number of equally spaced cylindrical shells, each with current I_i. with this method of sampling the current at each cylindrical shell of the uniform distribution beam is proportional to $(r_i^2-r_{i-1}^2)$.

For an e-beam with an initial Gaussian distribution, the beam at the entrance plane is assumed to be in its waist and the normalized Gaussian distribution function is given by

$$f_0(x,y,p_x,p_y)=\frac{1}{2\pi^2r_b^2p_b^2}\exp\left[-\left(\frac{x^2+y^2}{2r_b^2}+\frac{p_x^2+p_y^2}{p_b^2}\right)\right]. \tag{14}$$

The problem can be simplified by exploiting the azimuthal symmetry and transforming $f_0(x,y,p_x,p_y)$ into a cylindrical coordinates system resulting in the normalized distribution function

$$g_0(r,p_r,p_\theta)=\frac{r}{\pi r_b^2p_b^2}\exp\left[-\left(\frac{r^2}{2r_b^2}+\frac{p_r^2+p_\theta^2}{p_b^2}\right)\right]. \tag{15}$$

For proper sampling, distribution functions are divided into $N_t=N^3$ equal area segments where N is the number of macroparticles in a given dimension. One macroparticle is placed at the center of mass of each of the N equal area segments, as shown in Fig. 1.

In this sampling procedure each macroparticle carries the same portion of the beam charge, $I_i=I_b/N_t$. Consequently, the current in Eq. (12) becomes

$$I(r_i)=\frac{n(z)}{N_t}I_b, \tag{16}$$

where I_b is the total current in the beam, N_t the total number of macroparticles in the model, and n the number of macroparticles that are located below r_i. The expressions in Eqs. (12) and (16) are used for the calculation of the perveance as defined by Eq. (11), and substituted in the equation of motion (10). We note that the Gaussian canonical momentum distribution functions [Figs. 1(b) and 1(c)] are also used for the case of a beam with uniform distribution function in the radial dimension.

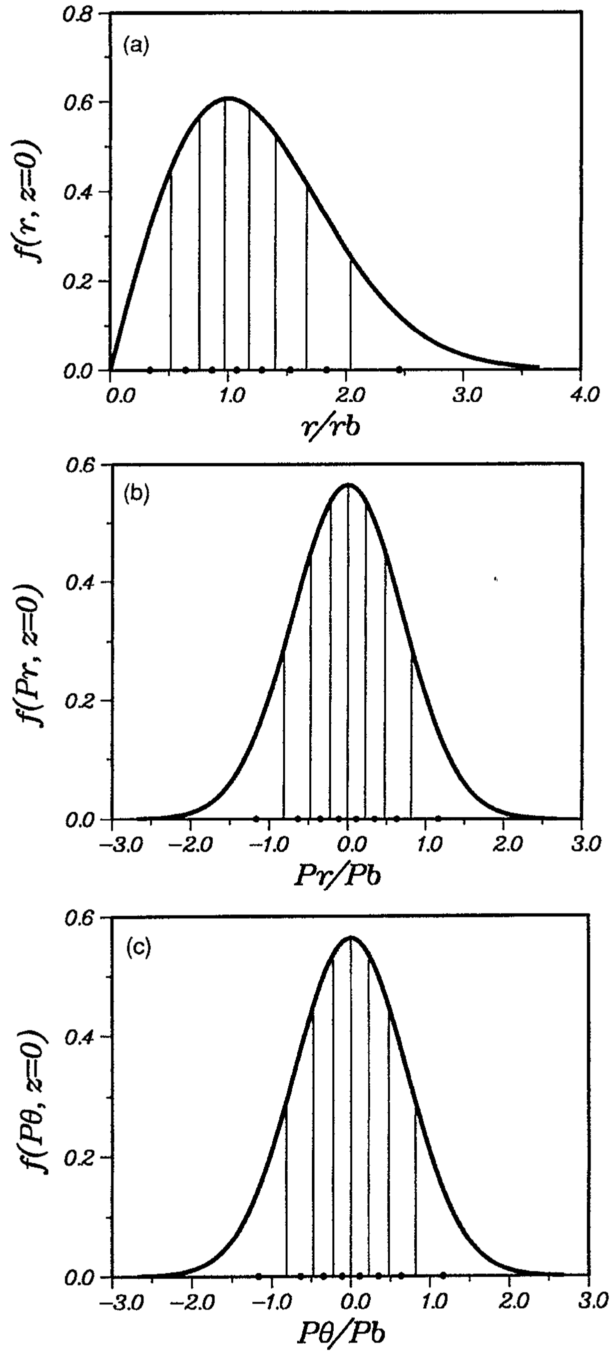

FIG. 1. The distribution functions were divided into N segments each of the same area. One macroparticle is placed at the center of gravity of each segment. Distribution functions shown are for (a) the radial dimension, (b) the radial momentum, and (c) the azimuthal momentum.

After calculating the trajectories of the sample macroparticles we need to find a way to recover a smooth current-density distribution out of the discrete spiky current-density distribution of the sample particles. Due to the azimuthal symmetry, the current I_i associated with each macroparticle located at r_i is distributed uniformly along a circular contour so that current density of this cylindrical shell current is given by

$$J_\lambda(x',y')=\frac{I_i}{2\pi r_i}\,\delta(\sqrt{x'^2+y'^2}-r_i). \tag{17}$$

This sampling current density can be turned into a smoothed current density function by converting it with an appropriate spread function, e.g., a Gaussian:

$$J_s(x,y)=\sum_{i=1}^{N_t}\frac{1}{\pi w_i^2}\int_{-\infty}^{\infty}\int_{-\infty}^{\infty}J_\lambda(x',y')\times\exp\left(-\frac{(x-x')^2+(y-y')^2}{w_i^2}\right)dx'\,dy'. \tag{18}$$

The width of the Gaussian spread function w_i is determined by a statistical criterion. One would expect that if the circle of radius w_i encompasses most of the electrons originating from the phase-space segment of the initial distribution represented by sample particle i, then the distribution due to the smoothing process is no greater than the loss of information produced by the sampling process. This loss of information can be reduced by increasing the number of sampling particles until the computed current-density distribution does not change.

After substituting Eq. (17) into Eq. (18) we get

$$J_s(r)=\frac{1}{2\pi}\sum_{i=1}^{N_t}\frac{I_i}{\pi w_i^2}\exp\left(-\frac{r^2+r_i^2}{w_i^2}\right)\times\int_0^{2\pi}\exp\left(\frac{2rr_i\cos(\phi'-\phi)}{w_i^2}\right)d\phi'. \tag{19}$$

Solving the integral in Eq. (19) gives the following result (which is as expected independent of ϕ):

$$J_s(r)=\sum_{i=1}^{N_t}\frac{I_i}{\pi w_i^2}\exp\left(-\frac{r^2+r_i^2}{w_i^2}\right)I_0(\mu_i r), \tag{20}$$

where $I_0(\mu_i r)$ is the modified Bessel function of the first kind with $\mu_i=2r_i/w_i^2$.

IV. PARTICLE TRAJECTORIES IN A SOLENOIDAL FIELD

The equation of motion is now slightly developed in order to solve a specific problem of e-beam transport in a solenoidal focusing magnetic field. Assume an axial magnetic field on-axis given by the analytical expression

$$B(0,z)=B_0\,\frac{\exp(-z^2/2b^2)}{1+z^2/a^2}, \tag{21}$$

where a and b are constant coefficients.[5,6] This distribution which models the field of an iron core solenoid axial magnetic field is plotted in Fig. 2.

The radial dependence of the focusing magnetic-field components can be approximated by a Taylor-series expansion, and expressed in terms of the axial field on-axis and its derivatives:[5]

$$B_z(r,z)\approx B(0,z)-(1/4)B''(0,z)r^2, \tag{22}$$

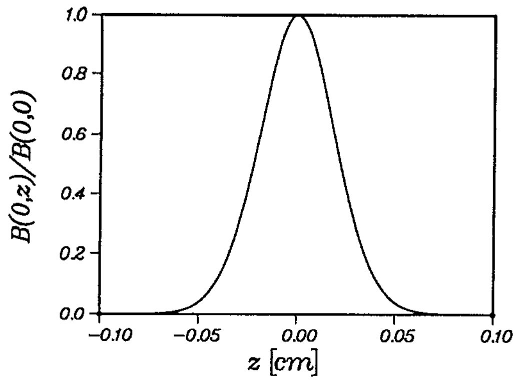

FIG. 2. The axial magnetic field along the z axis.

$$B_r(r,z) \approx -(1/2)B'(0,z)r + (1/16)B'''(0,z)r^3. \tag{23}$$

The above expansions of the magnetic field are substituted into Eq. (10) to get the radial equation for the electron trajectories,

$$r'' = -\left[\frac{\omega_L(z)}{c\beta_z}\right]^2 \left[1 - \frac{B''}{2B} r^2 - \frac{B'}{B} rr'\right] r - \frac{K(r)}{r} + \frac{\omega_L(z)}{\gamma mc^2 \beta_z^2}\left[\frac{B''}{4B} r + \frac{B'}{B} r'\right] L_{\theta_0} + \left[\frac{L_{\theta_0}}{\gamma mc\beta_z}\right]^2 \frac{1}{r^3}, \tag{24}$$

where $\omega_L(z) = eB(z)/2\gamma mc\beta_z$ is the local Larmor frequency. In this equation, third-order terms and higher are neglected. The axial velocity of the electron is determined from

$$\beta_z = \sqrt{1 - \frac{1}{\gamma^2}\left(1 + \frac{p_\theta^2 + p_r^2}{m^2c^2}\right)}, \tag{25}$$

where γ is constant. Eqs. (11), (12), (24), and (25) should solved simultaneously in order to simulate the electron trajectories and the beam behavior for a particular configuration. Note that Eq. (24) differs from the equation of motion which was derived in Ref. 5 by the last two extra terms in the rhs which are added to allow an initial canonical angular momentum spread in the beam which as, as shown subsequently, has an important effect.

V. SPACE-CHARGE EFFECTS

We solve numerically Eqs. (11), (12), (24), and (25) for the following parameters: a uniform 5 keV, 200 mA e-beam with a radius of $r_u = 20$ mm. The particles are launched parallel to the axis of a magnetic lens which is located at $z = 6$ cm. For studying the space-charge effects, zero initial canonical momentum spread is assumed ($L_{\theta_0} = 0$). In Figure 3(a) we present the trajectories in the case of no magnetic-field aberrations ($B' = B'' = 0$) and no space-charge forces. When aberrations are included ($B' \neq 0$, $B'' \neq 0$), particles cross the axis at different axial positions; thus the focus point is smeared out [Fig. 3(b)]. The outermost particle crosses the z axis before the others.

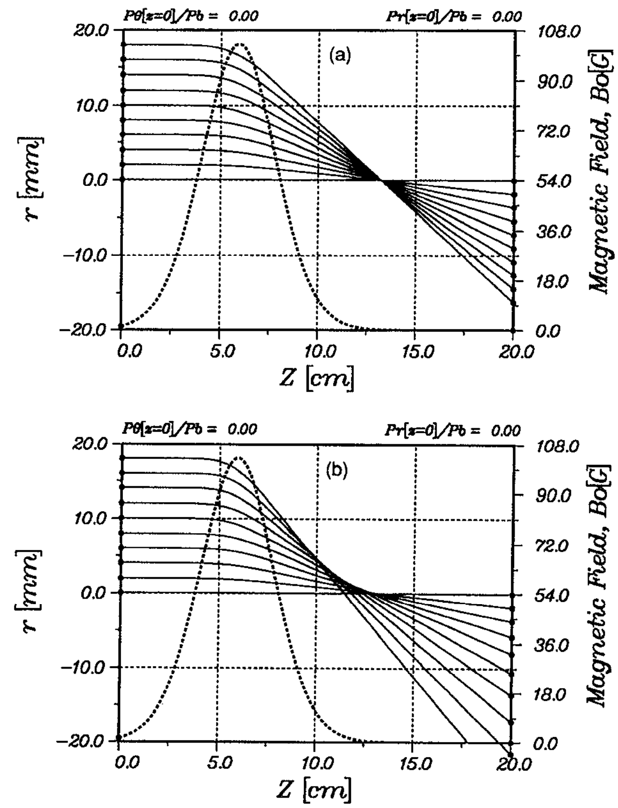

FIG. 3. Particle trajectories, in the absence of canonical momentum spread (for uniform current density): (a) without space-charge forces and field aberrations; (b) taking into account the field aberrations but still without space-charge forces. The dashed line represents the axial magnetic field.

For a uniform density current at $z = 0$, the e-beam perveance given in Eq. (24) is proportional to r^2. When the nonlinear terms in the first parentheses are negligible compared to unity, and in the absence of a canonical angular momentum spread, Eq. (24) simply includes two terms,

$$r'' = -\left[k_L^2(z) - \frac{k_p^2(z)}{2}\right] r, \tag{26}$$

where $k_p(z) = \omega_p(z)/v_z$ and $k_L(z) = \omega_L(z)/v_z$ are the plasma and Larmor wave numbers, respectively, with $\omega_p^2(z) = eJ_b(z)/\epsilon_0 \gamma \gamma_z^2 m v_z$. These linear forces are the magnetic-field force which tends to focus the beam and the space-charge force which repels the particles. Since the central forces behave like a linear pendulum with a constant restoring force for any $r < r_b$, particles in a monoenergetic beam which are launched parallel to the axis will follow scaled trajectories [i.e., at any z the ratio $r(z)/r_b(z)$=constant for each one of the particles in the beam] and thus will exhibit a laminar flow.[6] The electron beam (sampled in the simulation by 1600 macroparticles) is focused to a waist from which it diverges due to the high charge densities as shown in Fig. 4(a). The beam waist occurs at about 10 cm away from the lens center. We denote this distance by z_w. By adding field aberrations, some of the particles (the outermost ones) acquire radial momentum sufficient to overcome the space-charge repulsion and cross the

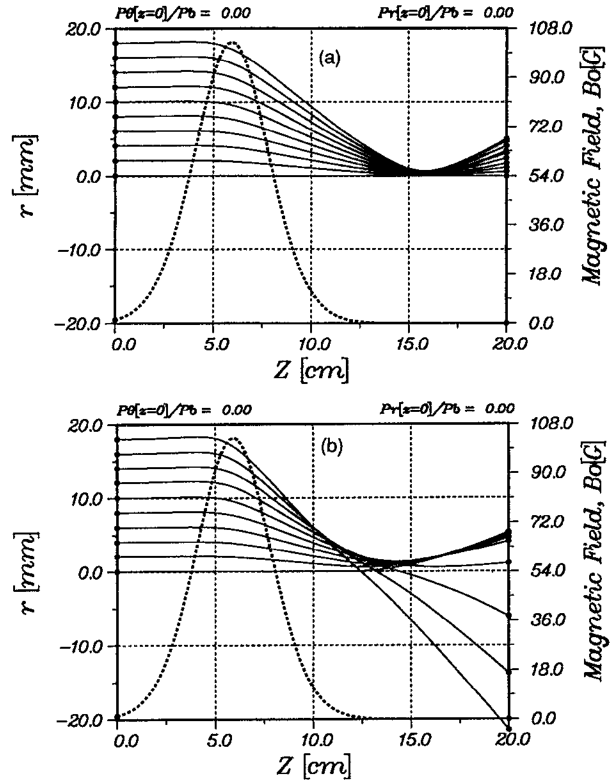

FIG. 4. Particle trajectories, in the absence of canonical momentum spread (for uniform current density): (a) including space-charge forces but with no field aberrations; (b) in the presence of both space-charge and aberration forces. The dashed line represents the axial magnetic field.

axis [Fig. 4(b)]. The beam waist is still located at z_w, and is surrounded by a weak halo. The particles that cross the axis contribute to this beam halo.

The current-density evolution is shown in Fig. 5. When the field aberrations are not included the beam is focused and

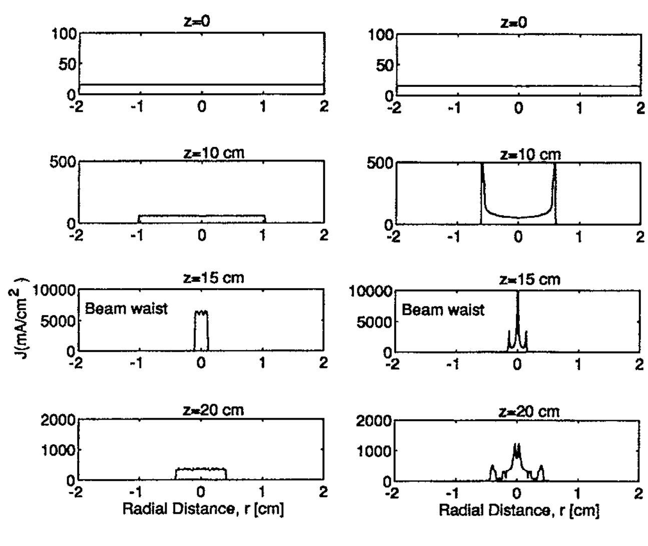

FIG. 5. The current-density evolution along the z axis for a beam with an initial uniform distribution function. The left column is obtained in the absence of field aberrations and in the right column they are included.

the current density reaches a maximum value at $z_w = 15$ cm. If the aberrations are taken into account, the current density in the beam cross section at $z = 10$ cm is high at its boundaries (the second plot on the right column of Fig. 5) due to the outermost particles which cross other particles trajectories. At $z = z_w = 15$ cm a very high current density appears on the axis and is surrounded by a halo.

Downstream the beam waist, at $z = 20$ cm, the beam expands and the peak current density decreases at the beam core, but the halo still exist around it. Another phenomenon that is observed in this case is the *phase-tearing* effect which was reported by Loschialpo *et al.*[5] In this effect the outermost particles cross the axis and the other particles change their radial positions in such a way that the ray order is inverted.

If the particles are not distributed uniformly, the space-charge force is not proportional to the radial distance r. For instance, if particles have initially a Gaussian distribution function, the space-charge force in the beam varies as $[1-\exp(-r^2/2r_b^2)]/r$ and achieves its maximum value at $r_c = 1.585 r_b$. For comparison purposes of the Gaussian beam and the uniform beam case, we define the effective radius of a Gaussian beam [r_b in Eq. (15)] to satisfy the same peak of intensity and total current as a uniform beam (a *top hat beam*), namely, $r_b = r_u/\sqrt{2}$. In the present examples, for a Gaussian beam we take at $z = 0$ a 5 keV, 200 mA e-beam with $r_b = 14.14$ mm. As was mentioned before, each macroparticle represents the same current fraction of the total beam current. The particle trajectories of a Gaussian e-beam passing through a thin magnetic lens in the absence of aberrations and with no initial canonical momentum spread are presented in Fig. 6. For the sake of clarity, we plot the trajectories in a radial range of $[-20,20]$ mm. The particles are launched from the entrance plane ($z = 0$) parallel to the axis, 6 cm behind the magnetic lens. Since the current density is not uniform, the space-charge force is not linear with r and hence the charge flow is not laminar as shown in Fig. 6(a). Many particles surmount the space-charge force and cross the axis. If lens aberrations are included [Fig. 6(b)], the radial slope of each particle becomes more tilted and the number of particles that overcome the space-charge repulsion force and cross the axis is increased. Particles which are initially located above r_c experience less space-charge repulsion than the inner ones. These particles acquire a radial momentum large enough to overcome the space-charge force, cross other trajectories, or even cross the axis.

The current density evolution for the Gaussian beam case is presented in Fig. 7. One can notice that if there are no aberrations (the left column plots of Fig. 7) the particles in the beam are still distributed Gaussianally even after passing the magnetic lens center, at $z = 10$ cm. At $z = z_w$ the particles that acquire a radial momentum large enough to cross the axis are responsible, in the present conditions, for the halo around the beam core. When the aberrations are taken into account (the right column plots of Fig. 7), the Gaussian current density soon changes its distribution and at $z = 10$ cm, 4 cm away from the magnetic lens center, a halo has begun to form around the beam core. It is found that at $z = z_w$ and away from this point, the beam cross section is more wide

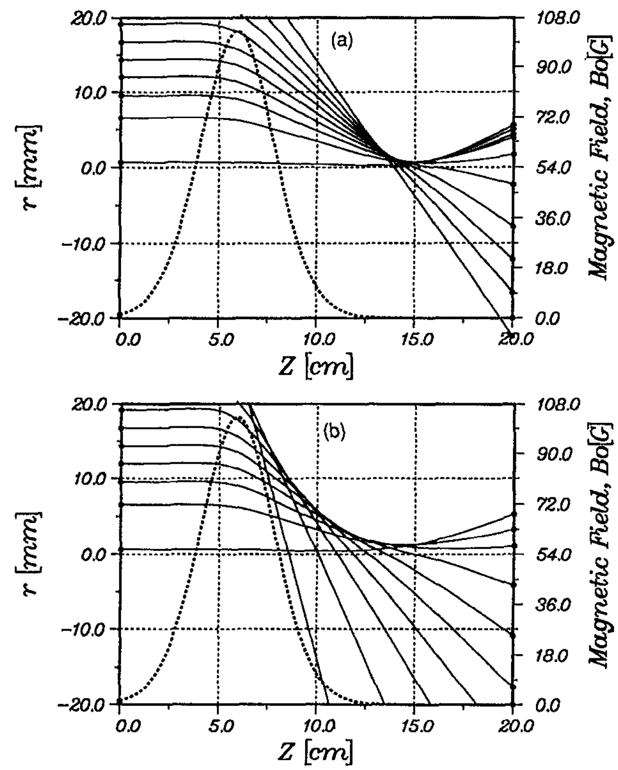

FIG. 6. Particle trajectories, in the absence of canonical momentum spread (for Gaussian current density): (a) taking into account space-charge forces but still without field aberrations; (b) in the presence of space-charge forces and field aberrations. The dashed line represents the axial magnetic field.

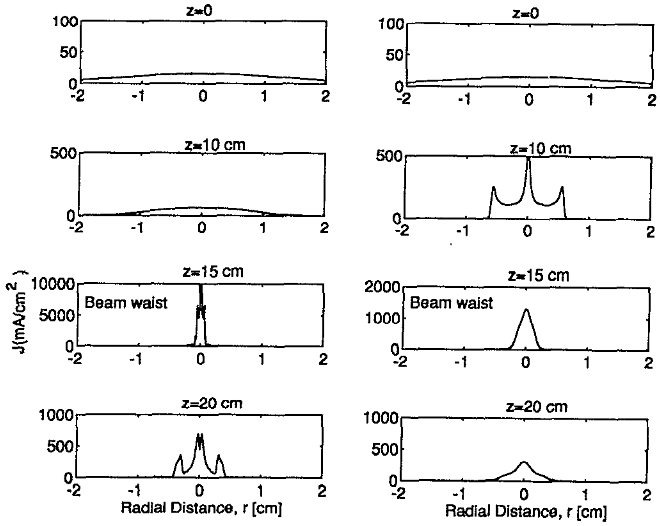

FIG. 7. The current-density evolution along the z axis for a beam with an initial Gaussian distribution function. The left column is obtained in the absence of field aberrations and in the right column the aberrations are included.

and the current density is a monotonic function of r, as shown in two last plots on the right column of Fig. 7.

VI. EFFECTS OF AZIMUTHAL AND RADIAL SPREADS OF CANONICAL MOMENTUM

In general, if a particle is launched with an initial canonical angular momentum, it will never cross the axis. When the e-beam has an azimuthal momentum spread, it prevents most of the particles from crossing the axis. The effect of the azimuthal and radial spreads of the canonical momentum can be best shown in phase space. We display a partial 2D phase space in which the coordinates are the radial position and the radial slope (r,r') of each particle trajectory in a given axial position. If the beam is azimuthally symmetric, as in the present model, the elliptical phase-space distribution is the same in any transverse direction, and we can define the emittance of the beam at the entrance plane as

$$\epsilon=\pi r_b \phi_{b\perp}, \tag{27}$$

where r_b is the beam waist radius and $\phi_{b\perp}=P_{b\perp}/P_z$ is the momentum spread half-opening angle. If we assume a transverse momentum spread of $\phi_{b\perp}=2$ mrad, then for the beam of radius $r_b=20$ mm this spread corresponds to a beam with emittance of 40π mm mrad. We simulated three different cases. In the first case the beam has no canonical momentum spread ($p_r=0$, $p_\theta=0$), in the second case the beam is assumed to have only an azimuthal canonical momentum spread ($p_r=0$, $p_\theta\neq 0$), and in the last case a radial canonical momentum spread is added ($p_r\neq 0$, $p_\theta\neq 0$). We simulate each of these cases for an e-beam which initially has a uniform or Gaussian charge distribution in the radial dimension. The e-beam and the magnetic lens parameters are the same as in the previous examples. We compare the phase space at three different points along the axis: before the beam waist position ($z=13$ cm$<z_w$), at the beam waist position ($z=z_w=15$ cm), and beyond the beam waist position ($z=20$ cm$>z_w$). In all three cases the aberration terms are included. For the sake of clarity we present in the phase-space plots only a diluted part of the total number of macroparticles that were simulated.

In Figs. 8 and 9 each point represents a single macroparticle. Figure 8 presents the results for an initially uniform beam distribution. The case where the beam contains no canonical momentum spread is shown in Figs. 8(a)–8(c). These results were already presented in real space in Fig. 4(b), and they agree with what was reported in Ref. 5 including a *phase-space tearing* effect. Note that in this singular case we permit r to assume negative values. In Figs. 8(d)–8(f) we add an azimuthal momentum spread to the beam. The consequence of this spread is a strong reflection of the particles away from the axis due to their centrifugal force. The particle trajectories are focused to a small radius spot centered on axis at $z=13$ cm which is closer than the beam waist position in the absence of azimuthal spread, z_w. No particle crosses the axis. At $z=15$ cm all the particles are already reflected and the beam expands. The inclusion of a radial momentum spread in the beam initial distribution [Figs. 8(g)–8(i)] causes the particle trajectories to be entirely reflected from the axis at a point which is even farther than $z=13$ cm and closer to the waist position z_w of the cold beam.

The phase-space evolution of a beam with an initially Gaussian distribution with no canonical momentum spread is depicted in Figs. 9(a)–9(c). These results are already shown in real space in Fig. 6(b). In the presence of azimuthal momentum spread in the beam, the particles which are not re-

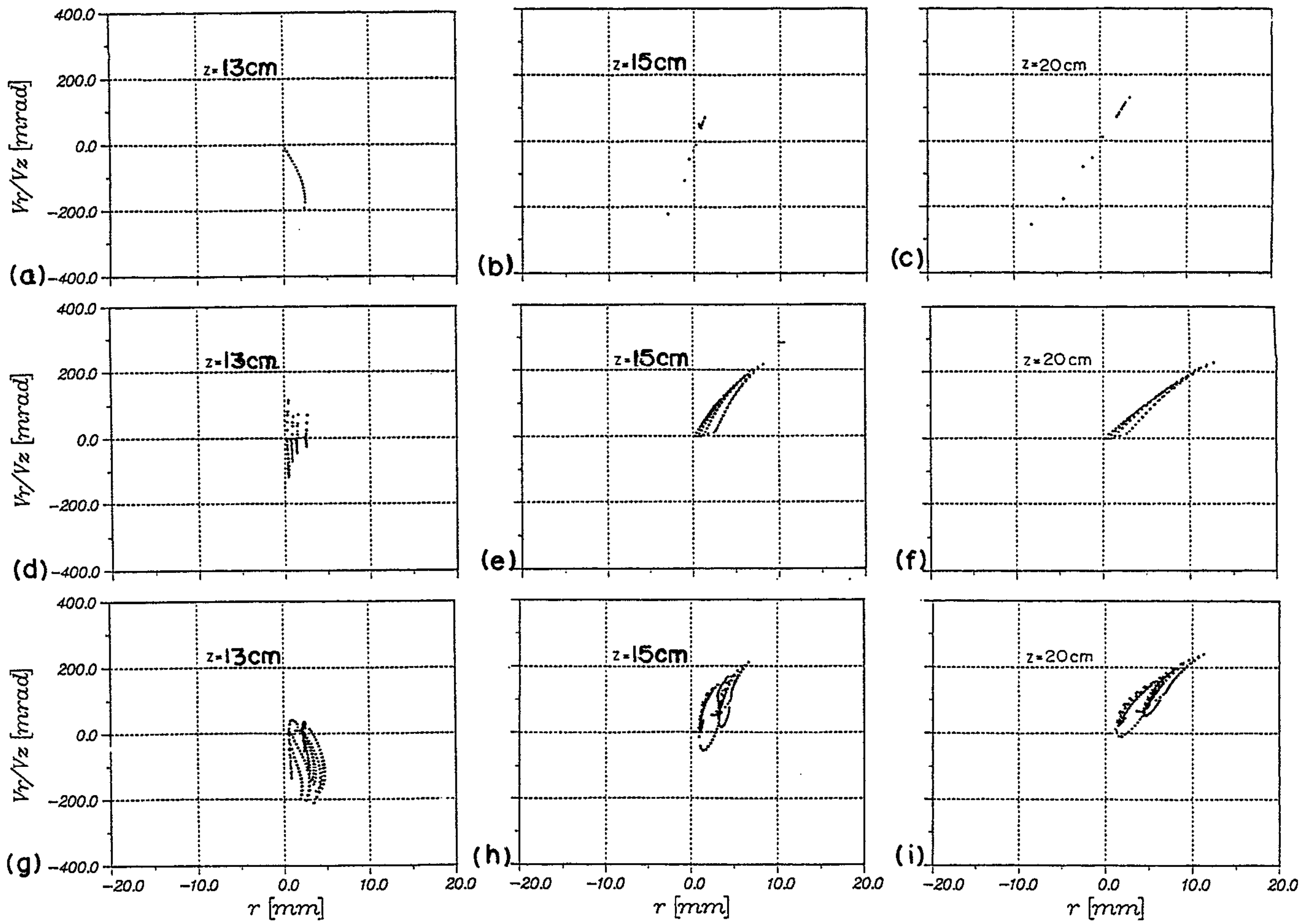

FIG. 8. Phase-space evolution for an e-beam with an initial uniform charge distribution at three distances along the axis: (a)–(c) without azimuthal and radial spreads, (d)–(f) including azimuthal momentum spread ($p_r=0$, $p_\theta \neq 0$), and (g)–(i) Including azimuthal and radial momentum spreads ($p_r \neq 0$, $p_\theta \neq 0$).

flected yet from the axis at $z=13$ cm [represented by the points in the fourth quadrant in Figs. 8(d) and 9(d)] are distributed the same as for the uniform beam case. However, there are much more particles that are reflected from the axis and the projected phase-space area is much larger than in the uniform beam case. The same effect is shown in Figs. 9(g)–9(i). From Figs. 8 and 9 it is clear that the effect of the azimuthal and radial spreads of the canonical momentum on the e-beam focusing characteristics is to produce a phase-space area growth and to prevent the phase-space tearing effect which was predicted by a model which does not include this spread.

Comparison of Fig. 9 to Fig. 8 indicates that there is an excessive growth in the *effective* phase-space area of the Gaussian beam as compared to the uniform distribution beam. This can be attributed mostly to the nonlinear space-charge defocusing effect which takes place with nonuniform electron current distribution. This is seen already at $z=13$ cm, for which even for the cold beam cases the Gaussian beam [Fig. 9(a)] exhibits larger canonical momentum spread and a highly nonlaminar flow, where the dots in the third quadrant in Fig. 9(a) correspond to electrons crossing the axis well before the waist position. There are no such electrons in the uniform current distribution case [Fig. 8(a)]. This excessive canonical momentum spread effect is even more pronounced in the case of a beam with initial canonical momentum distribution [Figs. 8(d)–8(i) and 9(d)–9(i)], where one notes that already at $z=13$ cm there are many more dots in the first quadrant (corresponding to diverging electrons) in the Gaussian beam case [Figs. 9(d) and 9(g)] than in the uniform beam case [Figs. 8(d) and 8(g)].

In comparison of the cold beam cases [Figs. 8(a)–8(c) and 9(a)–9(c)] to the canonical momentum spread cases [Figs. 8(d)–8(i) and 9(d)–9(i)] we note that in the latter case there are no electrons in the second and third quadrants. This is well understood from Eq. (24) which does not admit solutions for r which reverse sign for any z, as long as the centrifugal force (the fourth term in the equation) does not vanish. This tends to reduce dramatically the *phase-space tearing* effect predicted in Ref. 5 (namely, an abrupt disordering of the electron trajectories) because of two reasons: (a) much less electrons can arrive to the core of the beam near its axis and produce there an excessive space-charge force for the other electrons; (b) the effect of this excessive

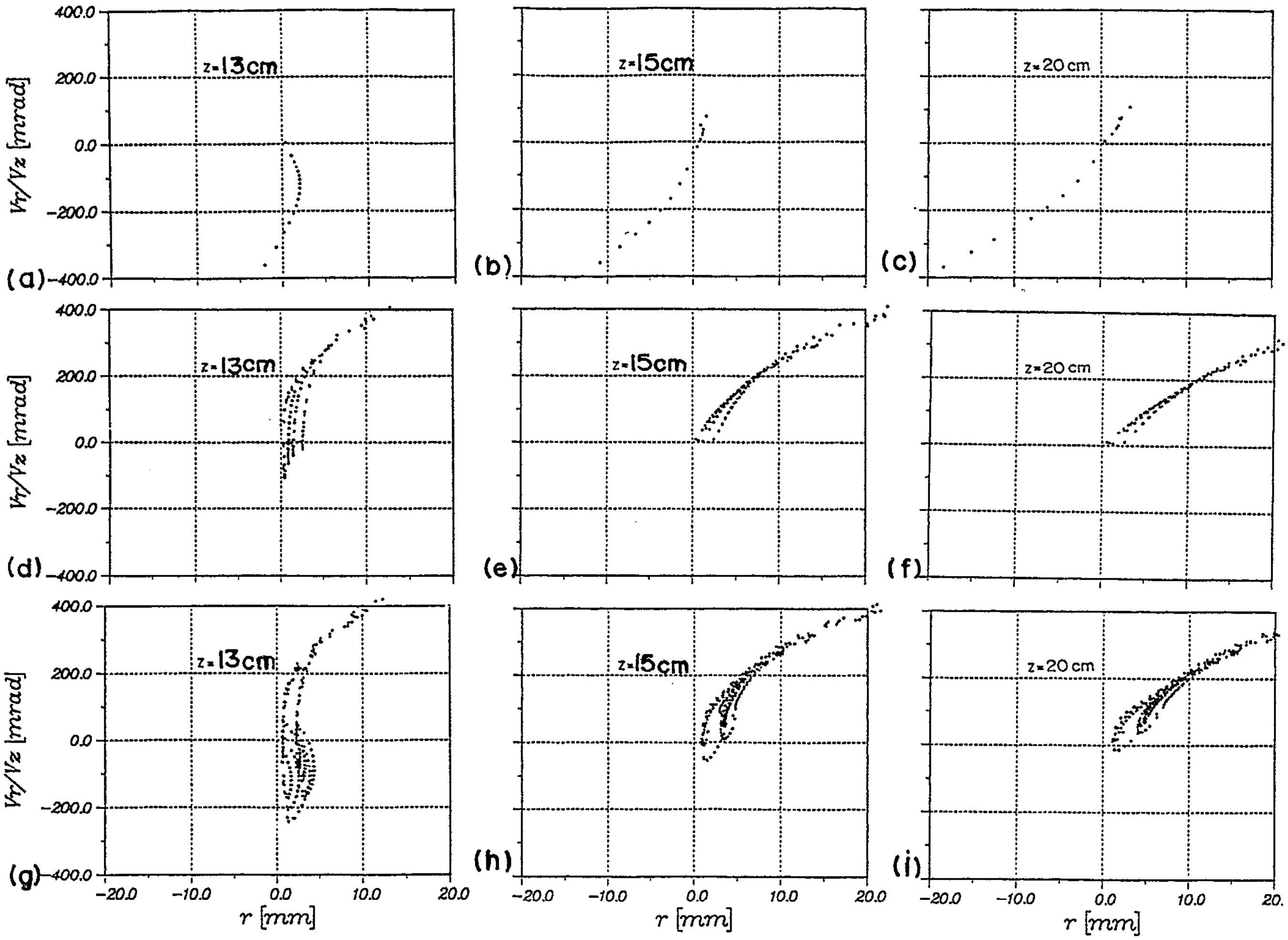

FIG. 9. Phase-space evolution for an e-beam with an initial Gaussian charge distribution at three distances along the axis: (a)–(c) in the absence of azimuthal and radial spreads, (d)–(f) with azimuthal momentum spread ($p_r=0$, $p_\theta \neq 0$), and (g)–(i) with azimuthal and radial momentum spreads ($p_r \neq 0$, $p_\theta \neq 0$).

space-charge force near the axis is small in comparison to the centrifugal force.

In Fig. 10 the current-density evolution in the presence of azimuthal canonical momentum spread for both uniform (left column plots) and Gaussian (right column plots) beams is presented. As was stated previously, the charge distribution at $z=13$ cm is similar for both distribution functions. The peak current density for an electron beam with canonical momentum spread is depressed. The shape of the current-density function is characterized by a concave form. Note at $z=15$ cm for the uniform case the beam has a strong halo surrounding a weak beam core, while for the Gaussian case the halo is nonexistent.

VII. CONCLUSION

The particle trajectories which are obtained by focusing of an electron beam which has an azimuthal and radial spreads of the canonical momentum differ from those obtained in a cold beam. This difference predicts for a *real beam* a current-density distribution which cannot be predicted by models that do not consider these spreads. We con-

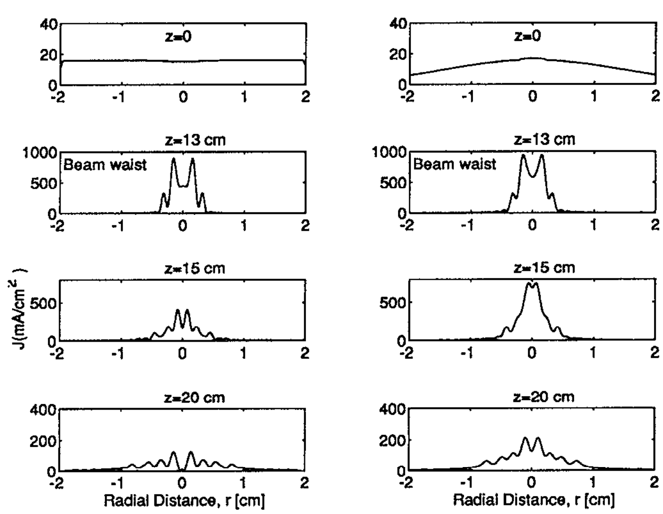

FIG. 10. The current-density evolution along the z axis in the presence of field aberrations and azimuthal momentum spread. Left column is obtained for a beam with an initial uniform distribution function. The right column is obtained for a beam with an initial Gaussian distribution function.

clude that inclusion of azimuthal and radial spreads of the canonical momentum (particularly azimuthal spread) in the simulation of beam focusing is quite vital for obtaining a reliable prediction of the current distribution profiles of the beam at the focus region and thereafter.

ACKNOWLEDGMENTS

This work was supported by the U.S.–Israel Bi-National Scientific Foundation, Israel Academy of Science and Ministry of Science.

[1] J. W. Gewartowski and H. A. Watson, in *Principles of Electron Tubes Including Grid-Controlled Tubes, Microwave Tubes, and Gas Tubes* (Van Nostrand, Princeton, NJ, 1965).
[2] H. P. Freund and T. M. Antonsen, in *Principles of Free Electron Lasers* (Macmillan, New York, 1992).
[3] J. C. Goldstein and B. E. Newnam, Nucl. Instrum. Methods A **318**, 349 (1991).
[4] J. Bengtsson and K. J. Kim, Nucl. Instrum. Methods A **318**, 344 (1991).
[5] P. Loschialpo, W. Namkung, M. Reiser, and J. D. Lawson, J. Appl. Phys. **57**, 10 (1985).
[6] J. D. Lawson, in *The Physics of Charged-Particle Beams* (Clarendon, Oxford, 1987), Chap. 3.